Journal of China University of Geosciences, *Vol. 15*, *No. 3*, *p. 283—289*, *September 2004* *ISSN 1002—0705*
Printed in China

Time-Frequency Variations of Plio-Pleistocene Foraminiferal Isotopes: A Case Study from Southern South China Sea*

Tian Jun Wang Pinxian Cheng Xinrong
Laboratory of Marine Geology, *Tongji University*, *Shanghai* 200092, *China*

ABSTRACT: The continuous wavelet transform (CWT) analysis reveals the instantaneous variability of the foraminiferal $\delta^{18}O$ and $\delta^{13}C$ of Site 1143 for the past 5 Ma at the eccentricity, obliquity and precession bands. The cross CWT analysis further demonstrates nonstationary phases of the benthic $-\delta^{18}O$ relative to ETP at the three primary Milankovitch bands in the last 5 Ma. The instantaneous phases between benthic $-\delta^{18}O$ and $\delta^{13}C$ at the precession band display a prominent 128 ka period, probably the cyclicity of the nonstationary climate close to the eccentricity. To explain these nonstationary phases, it is desirable to introduce a nonlinear response model to the global climate system, in which the output has a prominent cycle around 100 ka to match the 128 ka cycle of the instantaneous phase of the $\delta^{13}C$ and $-\delta^{18}O$ on the precession band.

KEY WORDS: wavelet analysis, foraminiferal, isotopes, South China Sea.

INTRODUCTION

The past thirty years have been important for proving the Milankovitch theory or the astronomical theory, which is an explanation for changes in the seasons which result from changes in the earth's orbit around the sun (Milankovitch, 1930). This theory has gained wide acceptance for its ability to account for two climate cycles: a 23 ka cycle that is phase-locked to the precession-driven insolation cycle, and a 41 ka cycle that is phase-locked to the obliquity-driven insolation cycle (Clemens and Tiedemann, 1997), although explaining the observed ~100 ka climate cycle in terms of Milankovitch theory, especially for the Late Pleistocene ice-age cycle, remains controversial in spite of a strong correlation with the ~100 ka cycle in the earth's orbital eccentricity (Imbrie et al., 1993). Test of this theory has often been performed on the frequency domain of the climatic time series, and the spectrum and cross spectrum analyses are the most acceptable methods, which actually generate mean results in a certain time interval. The flaw of these methods is that they can not identify the instantaneous intensity of a specific periodicity of a time series. To overcome this flaw, paleoceanographers accept another method, the continuous wavelet transform (CWT), to represent the traditional spectrum analysis. The CWT analysis has the ability of uncovering the instantaneous change of one component of a time series through time, revealing the time-frequency characteristics of the time series. In addition, it could also measure the instantaneous phases of one time series with another. By decomposing a time series into time-frequency space, one is able to determine both the dominant modes of variability and how those modes vary in time. Wavelet transform can be used to analyze time series that contains nonstationary power at many different frequencies (Torrence and Compo, 1998). Being influenced by the combined effects of incident radiation, global ice volume, continental biomass change, sea level change, sea water temperature and salinity variations, the time series of foraminifers' $\delta^{18}O$ and $\delta^{13}C$ contains nonstationary power at the major Milankovitch cycles, therefore the CWT analysis is the most

* This paper is supported by the National Natural Science Foundation of China (Nos. 40306011, 4999560 and 40321603) and the NKBRSF (No. G2000078500).

Manuscript received December 18, 2003.
Manuscript accepted March 10, 2004.

suitable tool to reveal the time-frequency characteristics embedded in these records.

MATERIALS AND METHODS

Two useful measurements to record marine sediment properties that could be linearly related to some index of climate are foraminiferal δ^{18}O and δ^{13}C, which in marine microfossils the former is approximately inversely proportional to the ice volume on land and the latter is proportional to the ocean carbon reservoir (Shackleton and Opdyke, 1973). In this study we utilize the benthic and planktonic foraminiferal δ^{18}O and δ^{13}C records from ODP Site 1143 to discuss the instantaneous response of the local climate change in the southern South China Sea (SCS) to orbital forcing.

A total of 1 992 samples of both benthic and planktonic foraminifers from upper 190.77 m at Site 1143 were measured for stable oxygen and carbon isotopes. The preparation of samples and stable isotope analyses were performed in the Laboratory of Marine Geology of Tongji University, Shanghai. The average time resolution of the samples is 2—3 ka. By taking the benthic foraminifer δ^{18}O as the tuning material and the obliquity and precession as the tuning target, a 5 Ma astronomical timescale for Site 1143 was established using an automatic orbital tuning method (Tian et al., 2002). After the astronomical tuning, the depth of 190.77 m from Site 1143 corresponds to an age of ~5 Ma.

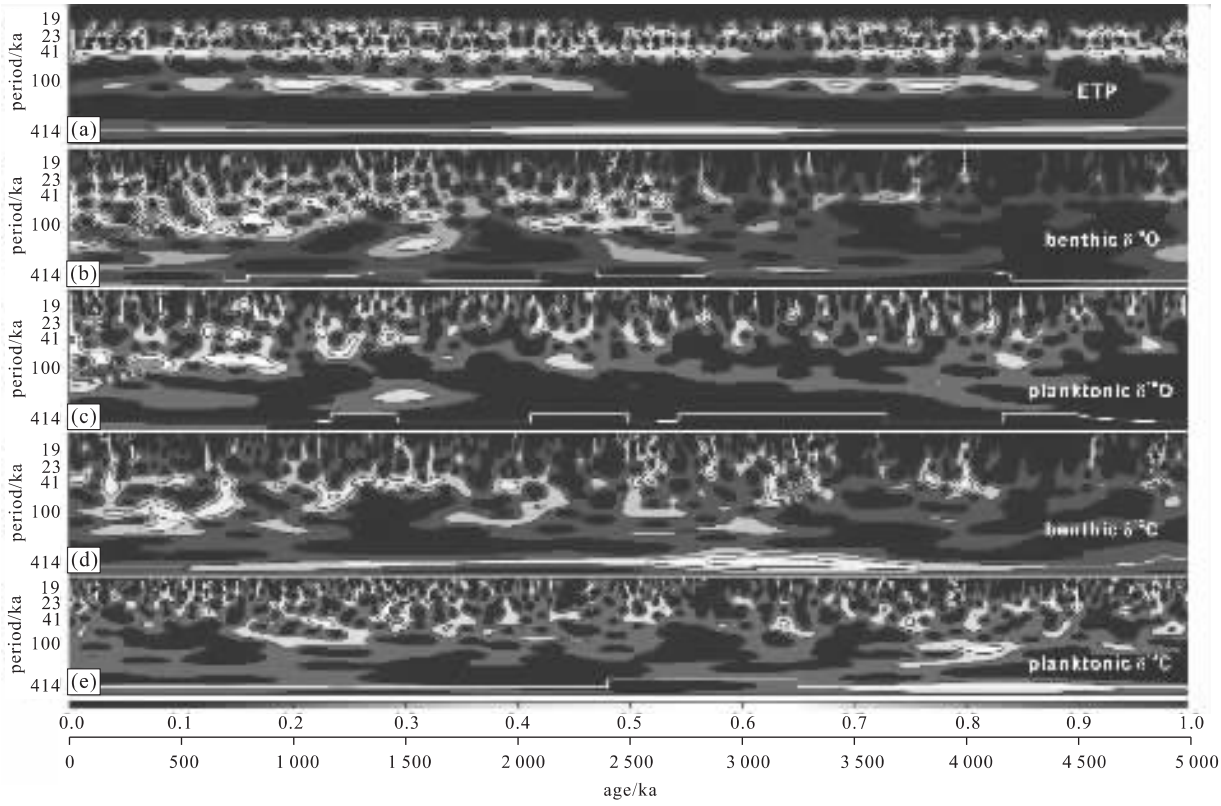

Figure 1. Modulus (standardized units) of the continuous wavelet transform of (a) Laskar90 (0,1) ETP (b) benthic δ^{18}O, (c) planktonic δ^{18}O, (d) benthic δ^{13}C and (e) planktonic δ^{13}C. The white lines are the ridges of the low-frequency around 1/414 ka. The bottom bar denotes the modulus (amplitude) density, with higher values indicating higher density.

TEMPORAL EVOLUTION OF PERIODIC ISOTOPES

CWT Analysis of Site 1143 Isotopes

The continuous wavelet transform (CWT) analyses were performed on four isotopic series from Site 1143 in the last 5 Ma, as shown in Fig. 1. For a comparison with the isotopic series, the CWT was also performed on Laskar90 (0,1) ETP. It is rather clear from Fig. 1a that most of the modulus power of the ETP is concentrated on the four Milankovitch bands, the 414 ka (periods from 360 to 460 ka), 100 ka (periods from 80 to 120 ka), 41 ka (periods from 36 to 46 ka) and 23 ka (periods from 17 to 25 ka), and

that the 41 and 23 ka cycles of the ETP are the most continuous in modulus power of the CWT throughout the last 5 Ma, followed by the 414 and 100 ka cycles.

Unlike the ETP, the moduli of the CWT of the isotopic series are not only concentrated on the four Milankovitch cycles, but also concentrated on some noisy periods. As seen from Fig. 1b, the 100 ka cycle of the benthic $\delta^{18}O$ is the most highlighted in amplitude in the last 0.4 Ma, followed by the time interval 0.4—1.0 Ma and 2.0—2.8 Ma. In the other time intervals, the 100 ka cycle is too weak to be noticed. The 414 ka cycle is too weak to be identified in the modulus of the CWT, whereas the 41 and 23 ka cycles are the most evident. The modulus of the CTW of the planktonic $\delta^{18}O$ is similar to that of the benthic $\delta^{18}O$, with a few differences with much stronger precessional components, as seen in Fig. 1c.

Compared with the benthic $\delta^{18}O$, throughout the last 5 Ma, the modulus of the 100, 41 and 23 ka cycles of the benthic $\delta^{13}C$ are weaker in the density, but the 414 ka modulus is extraordinarily strong, even stronger than the 414 ka cycle of the ETP, as seen in Fig. 1d. The 2.7—3.3 Ma interval is a period with the strongest modulus of the 414 ka cycle from the benthic $\delta^{13}C$. The modulus of the planktonic $\delta^{13}C$ also shows a great number of variances concentrated on the 414 ka band, though it is relatively weaker than the benthic $\delta^{13}C$ (Fig. 1e). Compared with the other three isotopic series, the 23 ka cycle of the planktonic $\delta^{13}C$ is the most powerful and continuous in modulus power.

Instantaneous Phase of ETP and Benthic $-\delta^{18}O$

The phase of two climate variables on a certain frequency band measured by cross spectrum is the average within a specific time interval, whereas that measured by cross CWT reveals the instantaneous change of the phase, as illustrated in Fig. 2.

On the obliquity band (Fig. 2b), the negative phase varies within a small range less than $\pi/2$ ($<90°$), with an average of -0.91 (in radian), approximately equal to 6 ka. In Fig. 2a, there are some

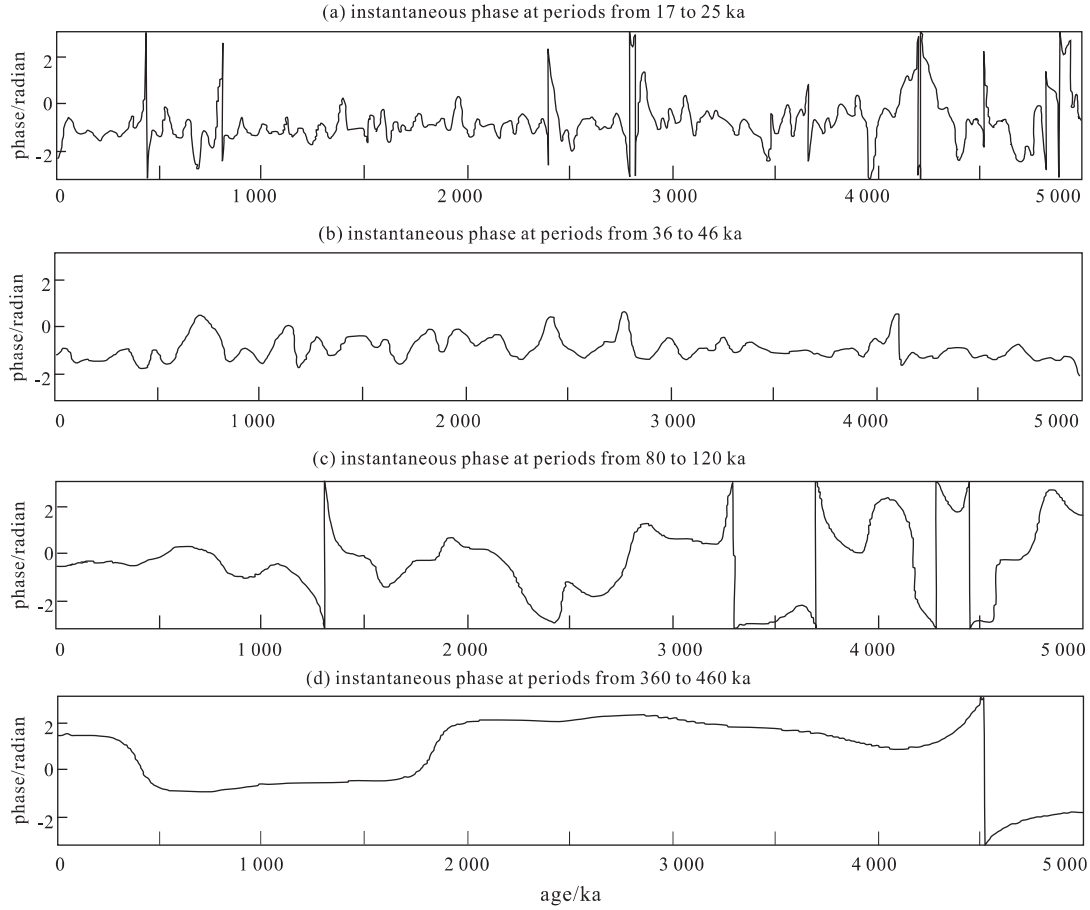

Figure 2. Instantaneous phase of the benthic $-\delta^{18}O$ relative to ETP at (a) periods from 17 to 25 ka, (b) periods from 36 to 46 ka, (c) periods from 80 to 120 ka and (d) periods from 360 to 460 ka.

abrupt shifts of the instantaneous phase at some specific time on the precession band, with an amplitude as much as π (≈90°), such as the time of 442, 810 and 4 212 ka. Usually, the abrupt phase shift had happened within two to five thousand years, then returned fast to the normal level. In addition, the mean instantaneous phase after 2.55 Ma is −0.97 (in radian), nearly two times the mean phase prior to 2.55 Ma. And also, the mean amplitude of the instantaneous phase is smaller after 2.55 Ma than that before this time. On the 100 ka eccentricity band, the instantaneous phase prior to ~1.5 Ma is generally nonstationary, with some abrupt shifts or long-term increase or decrease. It is just after 1.5 Ma that the instantaneous phase between the ETP and the benthic $-\delta^{18}O$ becomes stationary, keeping negative phases close to zero. The instantaneous phase on the 414 ka band is relatively stationary, with exceptions of big phase shift occurring at about 4.5 Ma and small phase shifts at 1.75 and 0.5 Ma.

Instantaneous Phase of Benthic $-\delta^{18}O$ and $\delta^{13}C$

As illustrated in Fig. 3a, the instantaneous phase of the benthic $-\delta^{18}O$ and $\delta^{13}C$ in the last 5 Ma on the precession band (periods from 17 to 25 ka) is the most nonstationary, interrupted by dozens of abrupt phase shifts. In general, the phase shift from positive to negative was abrupt or sharp, happened within several thousand years, and was then followed by a gradual increase. This periodic phase variation is like the Late Pleistocene $\delta^{18}O$ fluctuation, performing a dominant 128 ka cycle, as seen in Fig. 4.

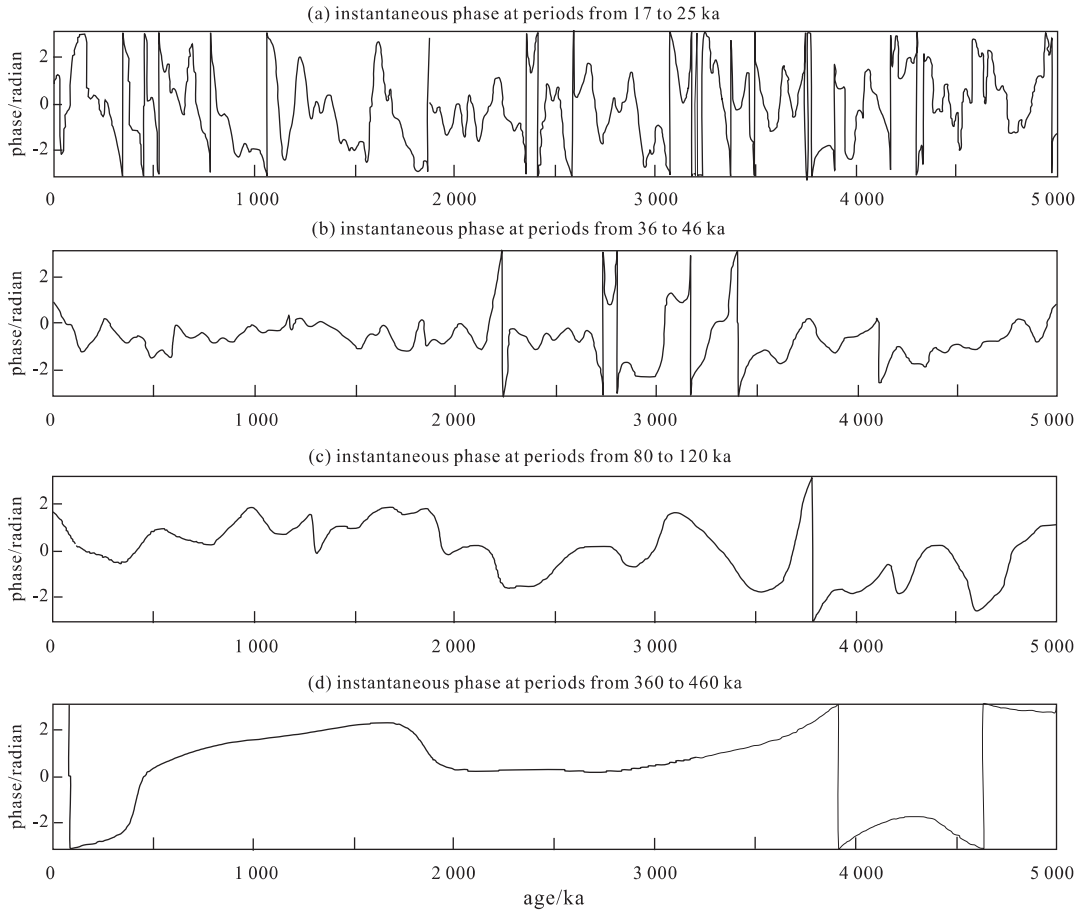

Figure 3. Instantaneous phase of $\delta^{13}C$ at (a) periods from 17 to 25 ka, (b) periods from 36 to 46 ka, (c) periods from 80 to 120 ka and (d) periods from 360 to 460 ka.

The instantaneous phase on the obliquity band (periods from 36 to 46 ka) is stable after ~2.2 Ma, varying in a small range less than π/2. Prior to 3.8 Ma, the instantaneous phase is also stable, varying in a small range, a little bit larger than the younger record after ~2.2 Ma. The time from ~3.8 to ~2.2 Ma is a nonstationary period for the instantaneous phase change, interrupted by four abrupt

phase shifts. Following the phase shift is a gradual decrease of the instantaneous phase, which is opposite to the post-phase-shift increase of the instantaneous phase on the precession band. On the whole, the instantaneous phase on the obliquity band is negative except for some short time intervals, indicating the leading variation of the $-\delta^{18}O$ relative to the $\delta^{13}C$.

On the eccentricity band (periods from 80 to 120 ka), there are two modes for the instantaneous phase change if ignoring some anomalies. One mode is the negative phase in relatively larger amplitude prior to ~2.2 Ma, and the second is the positive phase in relatively smaller amplitude after ~2.2 Ma. The instantaneous phase prior to ~2.2 Ma is also nonstationary when compared with that after ~2.2 Ma. This mode means that the variation of benthic $-\delta^{18}O$ leads that of benthic $\delta^{13}C$ prior to ~2.2 Ma on the eccentricity band, but lags after ~2.2 Ma. A sharp phase shift as much as π occurred at about 3.75 Ma, followed by a gradual decrease, similar to that on the obliquity band.

On the 414 ka eccentricity band (periods from 360 to 460 ka), the positive instantaneous phase is relatively stationary from ~3.9 to ~0.4 Ma. After 0.4 Ma, the instantaneous phase gradually decreases until ~0.1 Ma, and then abruptly changes to the positive level. At ~3.9 and ~4.15 Ma, there are also positive shifts of the instantaneous phase. In summary, on the low-frequency bands smaller than 1/100 ka, the benthic $\delta^{13}C$ usually leads the benthic $\delta^{18}O$ in the Late Pliocene and Pleistocene.

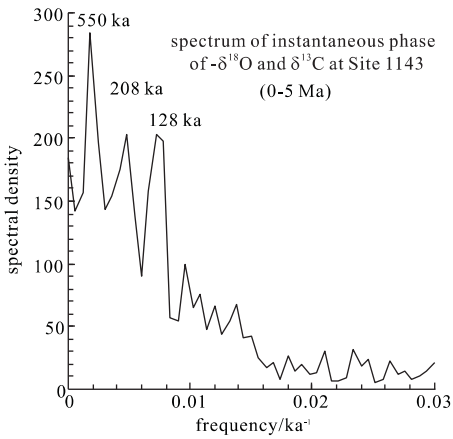

Figure 4. Spectrum of the instantaneous phase between the benthic $-\delta^{18}O$ and $\delta^{13}C$ from ODP Site 1143. The instantaneous is at the precession band (periods from 17 to 25 ka). The spectrum is performed using the ARAND software. The parameters are set as follows: t=1 ka; 5 000 data points; lag=2 000; autocovariance; linear detrend; variance=0.239 669; confidence level=80 %; band width=0.000 666; confidence intervals for spectral density: A1=0.564; A2=2.722.

DISCUSSION

The ocean holds the largest easily exchangeable carbon reservoir on earth, more than 50 times the carbon resident in the atmosphere (Broecker et al., 1980). Stable carbon isotope from benthic and planktonic foraminifera suggests that the distribution of carbon within the ocean controls atmospheric p_{CO_2} (Shackleton and Pisias, 1985). The benthic $\delta^{18}O$ can often be used to represent the global ice volume change. Therefore, clarifying the phase relationship between the benthic $\delta^{18}O$ and $\delta^{13}C$ can help find the mechanism which controls the p_{CO_2} change. The model developed by Imbrie (1985) may explain the observation that $\delta^{13}C$ lags $\delta^{18}O$ at shorter periods. The biosphere behaving in this model is taken as a simple exponential system responding with a single time constant. The phase of biomass relative to presumed forcing in this system is described by $\varphi = \arctan(2\pi f \tau_b)$, where φ is the phase angle at a given frequency; f is the frequency, and τ_b is the time constant for changing biomass. Such a model produces a phase shift, with great lags of the response behind the forcing at shorter periods. If the glaciation is taken as the climatic forcing of the biomass change, as recorded in the $\delta^{18}O$, the time constant of the changing biomass at obliquity and precession band can be simulated respectively by A1 and A2 as below

$$\tau_b(\text{obliquity}) = (41\ \text{ka}) * \tan\varphi/2\pi \quad (A1)$$

$$\tau_b(\text{precession}) = (23\ \text{ka}) * \tan\varphi/2\pi \quad (A2)$$

Table 1 lists the phase lag of the $\delta^{13}C$ relative to the $-\delta^{18}O$ in two time intervals, 0—2.5 Ma and 2.5—5.0 Ma. The time constant of τ_b (obliquity) and τ_b (precession) can be calculated by A1 and A2, as listed in Table 1. After 2.5 Ma, the time constant of the changing biomass is 3.2 ka and 3.3 ka for obliquity and precession bands respectively, whereas before 2.5 Ma, the time constant is 6.3 ka for the obliquity band and 2.1 ka for the precession band. The final initiation of the northern hemisphere ice sheet at about 2.75 Ma may have great impact on the biomass change, which led to the change of the time constant of the changing biomass. In general, the time constant of the changing biomass is around 2—3 ka, which is too long for living forest biomass which,

instead, should have responded by a factor of 10 times faster (Mix et al., 1995). Hence, changes in the mass of carbon in soils and shallow sediments must be involved to explain the 2—3 ka time constant, which would take longer to respond to the glaciation than the living forest. The Herbs% and *Pinus*% at Site 1144 of northern SCS in the last 400 ka lag the $\delta^{18}O$ by 17° and 23° respectively, at the obliquity and precession bands respectively (Sun et al., 2003). The variation of the pollen percentage reflects the vegetation change. According to A1 and A2, the time constant of the vegetation change is 2 ka for the obliquity band and 1.6 ka for the precession band. The 1—2 ka time constant of the vegetation change explains nearly 2/3 of the time constant of the changing biomass. Another time constant as much as 1—1.5 ka may come from the mass of carbon in soil and shallow sediments.

Table 1 Time constant of changing biomass in Imbrie's (1985) simple exponential system responding model

time interval	41 ka (obliquity)		23 ka (precession)	
	phase lag/(°)	time constant τ_b/ka	phase lag/(°)	time constant τ_b/ka
Q—2.5 Ma	26.2	3.2	41.9	3.3
2.5—5.0 Ma	43.2	6.13	29.8	2.1

Unfortunately, this simple exponential system responding model can not explain the lead of the benthic $\delta^{13}C$ relative to $-\delta^{18}O$. For example, the Herbs% and *Pinus*% at Site 1144 of northern SCS are coherent with the ice volume change at the eccentricity band in the last 400 ka, with nearly zero phases (Sun et al., 2003). This indicates that the 100 ka vegetation change in the continent of China is in phase with the 100 ka global ice volume change. If the model of Imbrie (1985) is true, this nearly zero phase could not explain the lead of the $\delta^{13}C$ relative to $-\delta^{18}O$. Therefore, a lead of $\delta^{13}C$ would require other climatic forcing of biomass unique to this band, which leads $-\delta^{18}O$ by nearly 20°, or the addition of another process such as changes in mean river $\delta^{13}C$ that could occur during climatic transitions (Mix et al., 1995). This process could reflect changes in chemical weathering which would only be expressed significantly by $\delta^{13}C$ at longer time scales, because of the longer residence time of carbon in the ocean. A study by Clemens et al. (1993) found that the $^{87}Sr/^{86}Sr$ change of the seawater has a 100 ka rhythm and leads ice-volume change at this band by about 20°. If the $^{87}Sr/^{86}Sr$ changes of the seawater really reflect the chemical weathering on the continent, this may explain the lead of $\delta^{13}C$ relative to $-\delta^{18}O$ on the eccentricity band.

The above discussion is based on the average phase within a specific time interval. If we use the instantaneous phase measured by the cross CWT analysis, as shown in Fig. 3, how can we explain the abrupt phase shift and the nonstationary phase, especially the frequent abrupt phase shifts on the precession band? To attribute this to the nonstationary time constant of the biomass seems to be unreasonable. It is therefore desirable to have a nonlinear response model, in which the output has a prominent cycle around 100 ka to match with the 128 ka cycle of the instantaneous phase of the $\delta^{13}C$ and $-\delta^{18}O$ on the precession band.

CONCLUSIONS

The CWT analysis reveals the instantaneous variability of the foraminiferal $\delta^{18}O$ and $\delta^{13}C$ of Site 1143 through time at the eccentricity, obliquity and precession bands. The cross CWT analysis further demonstrates nonstationary phases of the benthic $-\delta^{18}O$ relative to ETP at the three primary Milankovitch bands in the last 5 Ma. The instantaneous phases between benthic $-\delta^{18}O$ and $\delta^{13}C$ at the precession band display a prominent 128 ka period, probably the cyclicity of the nonstationary climate close to the eccentricity. To explain these nonstationary phases, it is desirable to introduce a nonlinear response model to the global climate system, in which the output has a prominent cycle around 100 ka to match the 128 ka cycle of the instantaneous phase of the $\delta^{13}C$ and $-\delta^{18}O$ on the precession band.

ACKNOWLEDGMENTS

This work was supported by the National Natural Science Foundation of China (Nos. 40306011, 4999560 and 40321603) and the NKBRSF (No. G2000078500). In particular we thank Dr. Wang Luejiang and his wife for sampling the 1143 cores. This research used samples and data provided by the Ocean Drilling Program (ODP). ODP is sponsored by the U. S. National Science Foundation (NSF) and

participating countries under management of Joint Oceanographic Institutions (JOI), Inc..

REFERENCES CITED

Broecker, W. S., Peng, T. H., Engh, R., 1980. Modeling the Carbon System. *Radiocarbon*, 22:565—598

Clemens, S. C., Farrell, J. W., Gromet, L. P., 1993. Synchronous Changes in Seawater Strontium Isotope Composition and Global Climate. *Nature*, 363:607—610

Clemens, S. C., Tiedemann, R., 1997. Eccentricity Forcing of Pliocene-Early Pleistocene Climate Revealed in a Marine Oxygen-Isotope Record. *Nature*, 385:801—804

Imbrie, J., 1985. A Theoretical Framework for the Pleistocene Ice Ages. *J. Geol. Soc. London*, 142:417—432

Imbrie, J., Berger, A., Boyle, E., et al., 1993. On the Structure and Origin of Major Glaciation Cycles, the 100 000-Year Cycle. *Paleoceanography*, 8:699—735

Milankovitch, M., 1930. Mathematische Klimalehre und astronomishe Theorie der Klimasch-Wankungen. In: Koppen, W., Geiger, R., eds., Handbuch der Klimatologie. Gebruder Borntraeger, Berlin. Ⅰ(A):1—76

Mix, A. C., Pisias, N. G., Rugh, W., et al., 1995. Benthic Foraminifer Stable Isotope Record from Site 849 (0—5 Ma): Local and Global Climate Changes. In: Pisias, N. G., Mayer, L. A., Janecek, T. R., et al., eds., *Proc. ODP Sci. Results*, 138:371—412

Shackleton, N. J., Opdyke, N. D., 1973. Oxygen Isotope and Paleomagnetic Stratigraphy of Equatorial Pacific Core V28-238: Oxygen Isotope Temperatures and Ice Volumes on a 105 Year and 106 Scale. *Quaternary Research*, 3:39—55

Shackleton, N. J., Pisias, N. G., 1985. Atmospheric Carbon Dioxide, Orbital Forcing, and Climate. In: Sundquist, E. T., Broecker, W. S., eds., The Carbon Cycle and Atmosphere CO_2: Natural Variations Archean to Present. *Geophys. Monogr. Ser., AGU, Washington, D. C.*, 32:313—318

Sun, X. J., Luo, Y. L., Huang, F., et al., 2003. Deep-Sea Pollen from the South China Sea: Pleistocene Indicators of East Asian Monsoon. *Marine Geology*, 201:97—118

Tian, J, Wang, P. X., Cheng, X. R., et al., 2002. Astronomically Tuned Plio-Pleistocene Benthic δ^{18}O Records from South China Sea and Atlantic-Pacific Comparison. *Earth and Planetary Science Letters*, 203:1015—1029

Torrence, C., Compo, G. P., 1998. A Practical Guide to Wavelet Analysis. *Bulletin of the American Meteorological Society*, 79:61—78